FEATURE ARTICLE

Imaging Surface Reactions at Atomic Resolution: A Wealth of Behavior on the Nanoscale

Xing-Cai Guo and Robert J. Madix*

Department of Chemical Engineering, Stanford University, Stanford, California 94305-5025

Received: August 29, 2002; In Final Form: November 5, 2002

In this feature article we review some of the striking results we have obtained with scanning tunneling microscopy (STM) on two single-crystal metal surfaces, Cu(110) and Ag(110), related to several general principles of surface reactions. While the "classic" surface science techniques are invaluable in providing supplementary information, STM has opened our eyes to the reality of the way in which surfaces participate in reactions. Simple adsorbates can form several nanometer-sized phases. Mixtures of reactants form cooperative structures that are far from homogeneous. Surface reactivity is site-specific and anisotropic. Step defects can have specific influences on reactivity. Reaction intermediates can inhibit the reactivity of the adsorbed reactants. The surface metal atoms rearrange in a manner far more complex than anticipated by the flexible surface model. We find that the reaction intermediates incorporate a stoichiometric number of metal atoms in the adsorbed layer, which leads to a significant amount of mass transport of metal atoms over the surface, altering the surface landscape. The alterable topography manifests itself as the formation of nanometer-sized islands or pits with a specific coverage. Such reaction-induced nano-restructuring has been observed for a number of reaction systems. The behavior of the surface in reactions is remarkably complex.

1. Introduction

The advent of scanning tunneling microscopy (STM) has opened our eyes to the reality of the way in which surfaces participate in reactions. It has become possible to image the surface directly at atomic resolutions and to witness the effects of reactions on the surface. In this article we will review some of the striking results we have obtained with STM on two single-crystal metal surfaces in our laboratory which relate to several general principles of reactions on surfaces. It was with such a vision in mind that we constructed our first variable temperature scanning tunneling microscope,[1] as described below in section 2.

The kinetics and mechanism of reactions on single-crystal metal surfaces has been the subject of intense study for nearly 30 years. Spawned from the desire to control the atomic structure and elemental composition of the surface in order to truly understand gas−surface interactions, such studies utilize low energy electron diffraction (LEED), Auger electron spectroscopy (AES) and/or X-ray or ultraviolet photoelectron spectroscopy (XPS or UPS) under ultrahigh vacuum (UHV) to ensure long-range order and purity (to about 1% level) of the surface, respectively. Most of the surfaces studied have been dominated by terraces of one crystal plane with well-defined structure. With the use of such defined surfaces and a myriad of surface-sensitive spectroscopic techniques, such as temperature programmed reaction spectroscopy (TPRS), high-resolution electron energy loss spectroscopy (HREELS), and infrared reflection absorption spectroscopy (IRAS), etc., it has been possible to identify and characterize a wide variety of adsorbed species and reaction intermediates on nearly all metals of chemical interest, including metals of groups IB, IIB and VIIIA of the periodic table. The adsorbed species and intermediates include oxygen, carbon, nitrogen, hydrogen, sulfur, carbon monoxide, carbon dioxide, nitric oxide, sulfur dioxide, nitrates, sulfates, carbonates, alkoxides, carboxylates, alkyls, alkylidynes, and π and di-σ bonded alkenes, etc. A general mechanistic understanding has been obtained for several classes of surface reactions. This approach is still very effective in elucidating complex surface reaction mechanisms, and the "classic" techniques continue to be invaluable in providing supplementary information necessary to understand the STM images of reactive systems, as exemplified in section 3 and throughout the text that follows.

The paradigms describing surface reaction kinetics are usually oversimplified, and STM has revealed complex interactions between reactants and reaction intermediates on surfaces. In general, the surface has been regarded as a two-dimensional homogeneous medium, and the concentration of reactants in the conventional rate equation has been taken to be a global average, i.e., the total number of adsorbed species of a given type per unit area, or in term of monolayers (ML, 1 ML is defined as one adsorbed species per surface atom). Reactions are generally assumed to occur between species in a well-mixed phase, similar to the state found in the gas or liquid phases. For example, second-order reactions are normally described as they are in the gas phase, the rate being proportional to the product of two global concentrations. The concept of a homogeneous reactant phase still dominates the thinking of surface reaction processes, although it has long been recognized that reactants may segregate into different phases on the surface, with reaction occurring at the phase boundaries. Simple adsorbates can form several adsorbed phases, some of which

* Corresponding author. E-mail: rjm@chemeng.stanford.edu. Fax: 650-723-9780.

10.1021/jp0219799 CCC: $25.00
Published on Web 02/01/2003

go undetected entirely by diffraction methods. Moreover, mixtures of reactants are observed with STM to form cooperative structures that are far from homogeneous. These phases may differ significantly in their reactivity or stability. In some cases STM reveals that reaction intermediates form structures that inhibit the reactivity of one or more of the adsorbed reactants. Anisotropic and site-specific reactivity as well as the effects of surface steps are clearly revealed. These matters are discussed in sections 4 and 5.

The "classic" point of view regarding the substrate surface is that the positions of the metal atoms remain essentially unperturbed with the formation of the bond to the adsorbed species. As surface diffraction methods were improved, however, it was found that the locations of atoms at the first layer of the surface differ from those expected from the undisturbed truncation of the bulk. The absence of bonding partners above the surface causes the outermost atoms to relax or reconstruct; there are also minor adjustments in the second and third atomic layers. The adsorption of strongly bound species may reduce the relaxation or induce further reconstruction. In many cases the atomic structure of the surface affected by adsorbed species, such as oxygen, sulfur, ethylene, and ethylidyne, has been determined from diffraction data. As a result of these studies, the concept of a "flexible surface" has been introduced, as opposed to the rigid surface.[2] For ethylidyne on Rh(111), for example, the spacing between the top and second layer metal atoms is increased by 0.1 Å compared to that of the clean surface. It is thus fair to say that, even relatively recently, single-crystal metal surfaces were regarded as consisting of a collection of steps, kinks, and terraces, with terrace sites dominating the surface, and adsorption could produce only minor rearrangement of this structure.

This picture of the surface in reactions is quite inadequate under many conditions, as we will show in section 6. Remarkably we find that the formation of metastable reaction intermediates involves the incorporation of metal atoms in the adsorbed layer, indicative of a stoichiometry of the adsorbed phase that may vary with the nature of the adsorbed species. As a result of this feature a significant amount of mass transport of metal atoms over the surface may occur during reaction. Surface restructuring is not limited to local rearrangements over a length scale that is a fraction of the lattice constant; it can alter the surface landscape on a nanometer scale. Thus, the surface not only has a flexible structure but also has an alterable topography. The surface alteration manifests itself as the formation of randomly distributed, nanometer-sized islands or pits on an otherwise flat terrace. This reaction-induced nanorestructuring has been observed for a number of systems where reaction intermediates incorporate metal atoms. The behavior of the metal surface in its reactions is rich with complexities heretofore undocumented.

Here we focus mainly on the ex situ STM observation of the surface as the result of reactions with ambient gases. A review of the in situ, real time STM observations of surface reactions is given elsewhere.[3] Our STM studies on metal oxide surfaces have been reviewed elsewhere recently.[4]

2. The Multitechnique Instrument and the Two Single Crystal Surfaces

At the time our variable temperature UHV STM instrument was built, most STM's required that the sample be placed on a stage, the temperature of which could not be controlled. Since we were interested in studying reactions and reaction intermediates it was imperative that the species of interest could be synthesized and stabilized for a period of time sufficiently long for imaging. We thus devised the instrument shown in Figure 1.[1] The key element in the instrument was the sample manipulator, which allows the sample to be positioned in front of several tools, each necessary for the identification and characterization of the adsorbed species. The STM is just one of the experimental elements of the instrument. The single-crystal sample can be moved from station to station while holding its temperature constant.

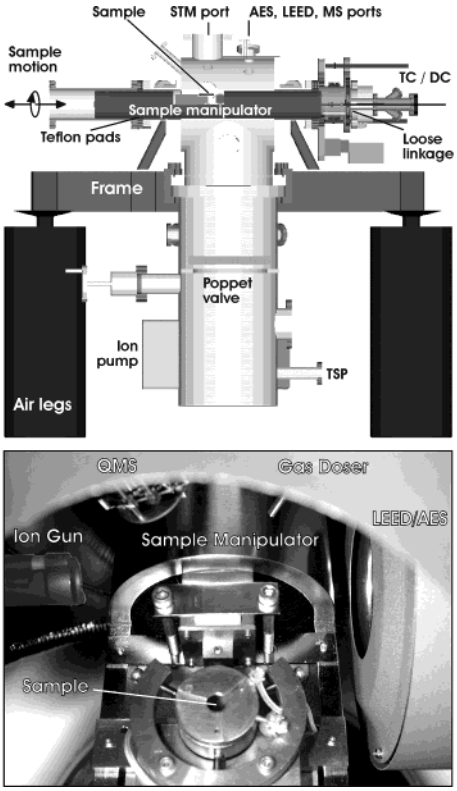

Figure 1. Our first variable temperature UHV STM instrument.[1] A photograph of the sample manipulator and various probes is shown at the bottom. (Section 2.) Reproduced with permission of the American Institute of Physics. Copyright 1995.

The studies described here were carried out on single crystals of silver and copper. Both single crystals (99.9999% purity) were aligned and cut to within 0.5° of the (110) plane and polished to a mirror finish. They were cleaned extensively with ion sputtering, annealing, and oxygen titration to remove traces of carbon. Their cleanliness was verified by various techniques, including Auger electron spectroscopy. Both crystals exhibited sharp LEED patterns, indicating good long-range order. An atom-resolved STM image of a small area of clean Ag(110) terrace is shown in Figure 2(a) along with a stacking-ball model (b).[5]

Some of the reactions reviewed here were carried out on oxygen-precovered surfaces. These surfaces were prepared by exposing the clean surface to pure oxygen gas (99.999%). The dissociative adsorption of O_2 on both Ag(110) and Cu(110) leads to the formation of a p(2×1)-O structure. An typical STM image of the atomic-oxygen-induced structure on Cu(110) is displayed in Figure 3a.[6] The round protrusions imaged in the chains running along the [001] direction are the copper atoms in the added −Cu−O− rows which form the well-ordered p(2×1)-O bands. The regions between the bands are clean surface where the copper atoms are unresolved. The added-row structure is well established and is depicted in Figure 3b. Oxygen atoms (small circles) reside in the short-bridge positions of the

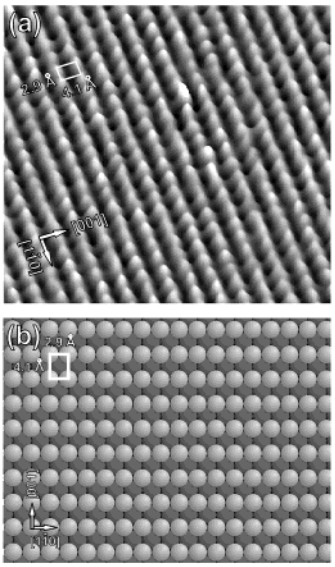

Figure 2. (a) An atom-resolved STM image of a small area of clean Ag(110) terrace, and (b) a stacking-ball model (b).[5] (Section 2.)

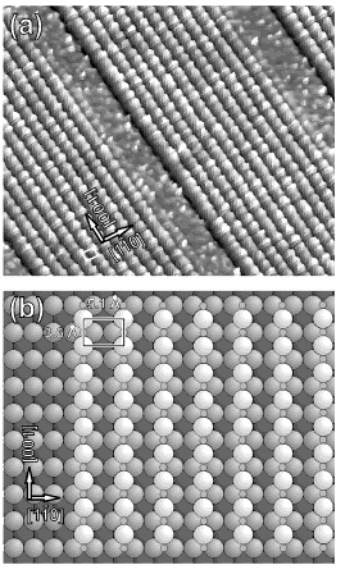

Figure 3. (a) An typical STM image of the atomic-oxygen-induced structure on Cu(110).[6] (b) A stacking-ball model of Cu(110)-p(2 × 1)-O with added −Cu−O− rows. The light, large circles represent the added layer of copper atoms, and the small gray circles are the oxygen atoms. (Section 2.) Reproduced with permission of the Royal Society of Chemistry. Copyright 1997.

underlying Cu layer. The local oxygen coverage within the p(2 × 1)-O bands is half a monolayer (0.5 ML, 1 ML = 1 O/Cu), though the total (global) coverage is less due to the presence of clean regions between the bands. The copper atoms incorporated into the added −Cu−O− row structure either diffuse from the terrace edges or are plucked from the terraces themselves to react with adsorbed oxygen atoms on the terraces. [7] The elucidation of this added row structure provided the first evidence of the incorporation of large numbers of "free" metal atoms into the structure of an adsorbate. Pitting was also noticed in the preparation of the Cu(110)-p(2 × 1)-O surface at low temperature or high O_2 pressure.[7]

The added row structure also forms on Ag(110), but the structural features of oxygen on Ag(110) and Cu(110) differ appreciably. Whereas on Cu(110) the −Cu−O− rows condense into uniformly spaced two-dimensional bands of the p(2 × 1)-O running for hundreds of Ångstroms across the surface, on Ag(110) two-dimensional condensation does not occur at low oxygen coverage, but form (n × 1) structures (n = 3−7), which stabilize into the p(2 × 1)-O structure at saturation coverage.[8,9] The difference in behavior of oxygen adsorption on Cu(110) and Ag(110) is not completely understood.

3. Substantial Supplementary Information Is Necessary in Order to Understand the STM Images of Reactive Systems

The scanning tunneling microscope provides images created by the overlap of the electronic states of the surface with those of the tip. As of today, STM alone does not provide sufficient information to identify the species imaged. Thus, it is imperative that other methods are used to establish the identity of the species under study. Useful methods for this purpose include temperature programmed reaction spectroscopy (TPRS), X-ray photoelectron spectroscopy (XPS) and vibrational spectroscopy. A good example of this interplay is the studies of carbonate on Ag(110).

3.1. Carbonate versus Carbon Dioxide on Ag(110).[5,10] As a result of extensive study by TPRS, XPS, UPS, its near-edge absorption X-ray fine structure (NEXAFS), HREELS, and IRAS, it has been shown that reaction between CO_2 and O(a) on Ag(110) produces a two-dimensionally ordered surface carbonate.[11−22] A particularly important characteristic of this carbonate is that it yields CO_2(g) at 475 K and O_2(g) near 600 K when heated. In 1995 three research groups, [23−25] following the recipes for carbonate formation described in the original papers, obtained beautiful STM images which they attributed to the surface carbonate species, CO_3(a). These studies raised a controversy over the simple 1:1 reaction stoichiometry between CO_2:O(a) reported for carbonate formation in the previous work,[11] because the relative number of features in the STM images attributed to the reactant, adsorbed oxygen, and the product carbonate were clearly at variance with this ratio.[23] Because this reaction is relatively simple, the apparent complexity of the stoichiometry for this reaction suggested by STM gave cause for concern about the state of understanding of even the simplest reactions.

In investigating this problem further we obtained STM images with features essentially identical to those attributed to carbonate in the recent work (Figure 4a). Heating this surface (a TPRS measurement), however, yielded only a CO_2 peak at 475 K, as shown in Figure 4b; no O_2 near 600 K was observed. The absence of the accompanying O_2 desorption peak from the surface pictured in Figure 4a indicates that it was not carbonate imaged in theses three studies, but *chemisorbed* carbon dioxide, CO_2(a). Further study reveals that this unusual state of CO_2(a) is formed by the reaction of CO(g) present in the ultrahigh vacuum background with the carbonate.[5] This chemisorbed species appears to be stabilized by the (1 × 2) reconstruction of the silver atoms in the (110) surface that accompanies carbonate formation. Thus the *combination* of TPRS and STM resulted in the discovery of the rather unusual *chemisorbed* CO_2 state on Ag(110), and actually allowed the 1:1 reaction stoichiometry of CO_2 and O(a) for carbonate formation to be proven.

The carbonate actually appears as thick rods in STM (Figure 4c). Its identity is verified by the TPR spectra taken subsequently shown in Figure 4d. The peak temperature and peak shape of both CO_2 and O_2 are identical to those obtained previously for carbonate decomposition.[11] On the bases of high-resolution STM images, a structural model has been suggested with the surface carbonate species sitting on a top-layer Ag atom next to two

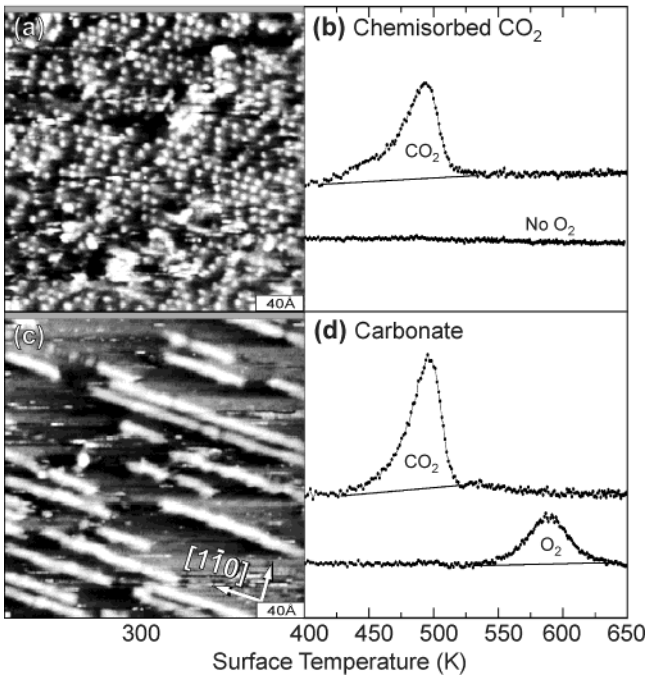

Figure 4. STM images of (a) chemisorbed CO_2 and (c) carbonate on Ag(110). Frames (b) and (d) show temperature programmed desorption traces resulting from heating the two different surfaces at 2 K/s.[5,10] (Section 3.1.) Reproduced with permission of Elsevier. Copyright 2001.

added Ag atoms in a slightly tilted orientation on a reconstructed Ag(110)−(1 × 2) surface.[10]

4. Temperature-Dependent, Site-Specific Reactivity of Surface Oxygen in Different States of Aggregation

Scanning tunneling microscopy affords the opportunity to observe reactions of adsorbed species, either with one reactant preadsorbed and another present as a gas or with both present in the gas phase. In the first condition the surface concentration of the preadsorbed reactant will be depleted in a transient fashion; in the second condition a steady state will be reached in the surface concentration of both species. On Cu(110) oxygen forms short, isolated −Cu−O− rows at low oxygen coverages, which aggregate into the p(2 × 1)-O bands at high coverages (cf. Figure 3). Prior to its reaction with mobile copper atoms to form these rows, oxygen exists in a transient, metastable reactive state.[26] Because these states of oxygen differ appreciably in their binding energy to the surface, one would expect them to exhibit different reactivities. We have investigated the reactivity of oxygen in these three forms toward CO (oxidation) and NH_3 (oxydehydrogenation) between 150 and 400 K with our variable-temperature STM.[1] At 150 K only the transient oxygen is reactive with CO, and at 300−400 K all forms of oxygen are reactive with CO. At 300 K isolated −Cu−O− rows exhibit reactivity similar to the transient oxygen for NH_3 oxydehydrogenation. The boundaries and inner regions of p(2 × 1)-O bands only become reactive at elevated temperatures. The reactivity of oxygen clearly depends on its state of two-dimensional aggregation. Site specificity and reaction anisotropy is also observed near steps.

4.1. Highly Reactive Oxygen Transients for CO Oxidation on Cu(110) at 150 K.[27] When the Cu(110) surface is precovered with p(2 × 1)-O, exposure to CO at 150 K produces no reaction between CO(g) and O(a). Instead, CO simply adsorbs in regularly spaced stripes on the clean surface regions, spanning the bands of p(2 × 1)-O. Shown in Figure 5 are four STM

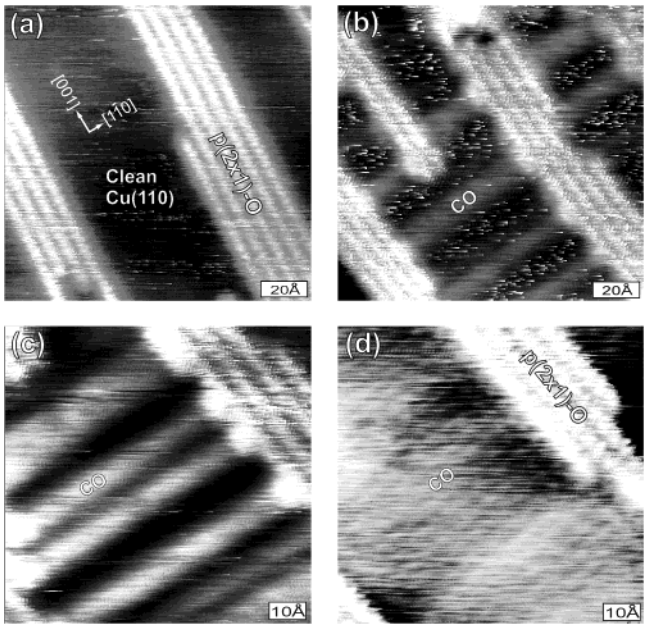

Figure 5. Sequential STM images obtained at 150 K during CO exposure on Cu(110) preadsorbed with atomic oxygen.[27] (Section 4.1.) Reproduced with permission of Elsevier. Copyright 1996.

images obtained during CO exposure at 150 K. Figure 5(a) shows the surface partly covered with p(2 × 1)-O at 150 K, as prepared with oxygen exposure at 300 K and annealing to 450 K. Figure 5b shows an image obtained immediately after beginning CO exposure. Faint stripes perpendicular to and spanning the p(2 × 1)-O bands are attributed the adsorbed CO. Figure 5c shows a zoomed-in image of the same region after continued CO exposure. The CO stripes have broadened significantly. After a saturation exposure a compressed CO structure is formed (Figure 5d). The CO structure remains in contact with the p(2 × 1)-O structure without reaction. Similarly, CO does not react with isolated, short −Cu−O− rows at 150 K. The lack of reactivity may be due to the immobility of −Cu−O− rows at such a low temperature.

On the other hand, when the surface, partly covered with p(2 × 1)-O and CO(a) stripes, is exposed to O_2(g), the CO(a) stripes disappear from the STM images, and at the same time CO_2 is evolved into the gas phase.[27] This indicates that at 150 K the only reactive oxygen species is a transient form which has not yet reacted with mobile copper atoms to form either short −Cu−O− rows or to extend the p(2 × 1)-O boundaries, which supports the suggestions made early.[26]

4.2. Anisotropic Reactivity of p(2 × 1)-O for CO Oxidation on Cu(110) at 400 K.[28,29] Although unreactive at 150 K (Section 4.1), the p(2 × 1)-O bands on Cu(110) are reactive with CO at 400 K. Figure 6 shows a series of STM images of the same region taken 2.5 min apart during exposure of the preoxidized surface to CO at 400 K. Clearly, the oxygen rows on the perimeter of p(2 × 1)-O bands react away one by one in a sequential manner. The p(2 × 1)-O band becomes thinner and thinner, as indicated by the two arrows, and finally disappears (Frame 05), leaving a clean Cu(110) surface. Ultimately a clean surface is produced at 400 K (Frames 05 and 06). The STM images from Frame 01 to 04 show only the oxygen added row structure; CO is not imaged due to its short lifetime ($\sim 10^{-6}$ s), its low equilibrium coverage ($\sim 10^{-4}$ ML), and its high mobility at 400 K. CO_2 desorbs from the surface upon formation at this temperature. Comparison of the observed p(2 × 1)-O band shapes to those from Monte Carlo simulations

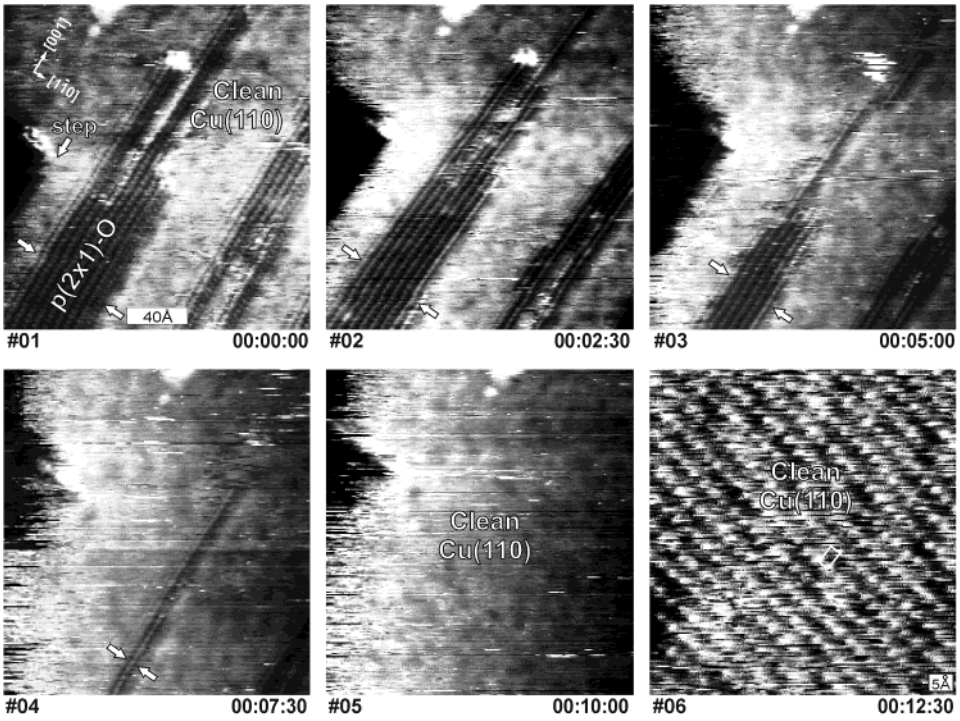

Figure 6. Sequential STM images obtained at 400 K for the same region during CO oxidation on Cu(110) preadsorbed with atomic oxygen.[28,29] (Section 4.2.) Reproduced with permission of Elsevier. Copyrights 1994 and 1996.

suggests that the reaction probability at the end of a row is 500−1000 times greater than that at the side of a band. The highly anisotropic reactivity of oxygen is similar to that observed near room temperature for CO oxidation on Rh(110),[30] and methanol oxidation on Cu(110).[31]

4.3. Reactivity of Various Oxygen Forms for NH_3 Oxydehydrogenation on Cu(110).[32] The reactivity of the forms of oxygen on Cu(110) with ammonia has been investigated quantitatively by in situ STM at 300 K. Both the p(2 × 1)-O bands and isolated −Cu−O− rows react with ammonia to form H_2O(g) and NH(a) at 300 K. At low oxygen coverages the isolated −Cu−O− rows are consumed readily, while at high coverages reaction proceeds from the boundaries of p(2 × 1)-O bands. Though the reaction can be initiated from both the end and the side of the −Cu−O− rows, the reactivity again appears to be anisotropic, being higher along the [001] direction. This feature is illustrated by STM images obtained sequentially as the reaction proceeds (Figure 7). The NH(a) structures appear as thick, beaded rows orthogonal to the −Cu−O− rows. Under an ammonia pressure of 2×10^{-9} Torr, two −Cu−O− rows in the perimeter of a p(2 × 1)-O band are reacted away progressively, as indicated by arrows 1 and 2 in Frames 01 through 05. An opening in the middle of a −Cu−O row is created in Frame 04 (arrow 4), which widens in the following frames (arrows 4 and 5). By direct counting of the atoms in STM images it was possible to show that the reactivity of transient oxygen species is comparable to that of the isolated −Cu−O rows, both of which are more reactive than oxygen at the perimeters of the p(2 × 1)-O bands.

4.4. Effect of Step Defects: NH_3 Oxydehydrogenation on Cu(110).[33] Defects on surfaces, such as steps, are thought to influence catalytic activity considerably, but few microscopic observations have been made on their effects. We have shown by STM that step defects have a strong effect on the reactivity of oxygen toward NH_3. Furthermore, the reactivity at steps can differ according to their crystallographic orientation. Reactivity of O(a) on Cu(110) toward ammonia is high at the top and bottom of a step running in the $[1\bar{1}0]$ direction and at the bottom of a [001] step, whereas almost no reaction occurs at the sites bordering the top of a [001] step. Figure 8a displays a large section of the surface with a monatomic $[1\bar{1}0]$ step indicated at the left-hand side of the image. The darker bands along the [001] direction are p(2 × 1)-O structures. Before reaction the oxygen bands extended uninterrupted across the step edges. Clearly, oxygen atoms at the ends of the bands, all of which were terminated at the $[1\bar{1}0]$ step, have been reacted away from both sides of the step. The reactions create fork-like ends in the remaining p(2 × 1)-O structures (dark). These distinct terminations of the p(2 × 1) bands are caused by the intrusion of rows of NH(a) which run orthogonal to the −Cu−O− rows (see the inset in Figure 8a), which terminate the −Cu−O− string and inhibit it to further reaction along the [001] direction.

Figure 8b shows terraces separated by [001] steps of monatomic height. The oxygen rows near the bottom of these steps have reacted most extensively, whereas the oxygen rows at the top of the [001] steps show little reactivity. Reaction at the bottom of [001] steps leads to deposition of Cu atoms released from the −Cu−O− rows, and thereby extends the step edges.

4.5. Site-Blocking Inhibition Effects: NH_3 Oxydehydrogenation on Cu(110) and Ag(110).[6,34] As noted above, our studies of ammonia oxidation with scanning tunneling microscopy have shown that the formation of reaction intermediates can poison further reaction. Self-organized spatial patterns of coadsorbates have been observed during ammonia dehydrogenation reactions, which illustrate inhibition due to site blocking by the accumulation of a reactive intermediate on the surface for the ammonia-oxygen system. Figure 9a,b shows complex two-dimensional configurations formed by −Cu−O− rows and NH(a) structures after annealing coadsorbed NH_3 + O on Cu(110) to 410 K. An isolated −Cu−O− row of 53 Cu atoms is seen in Figure 9a with both of its ends blocked by NH(a) structures. Numerous shorter, otherwise reactive −Cu−O− rows

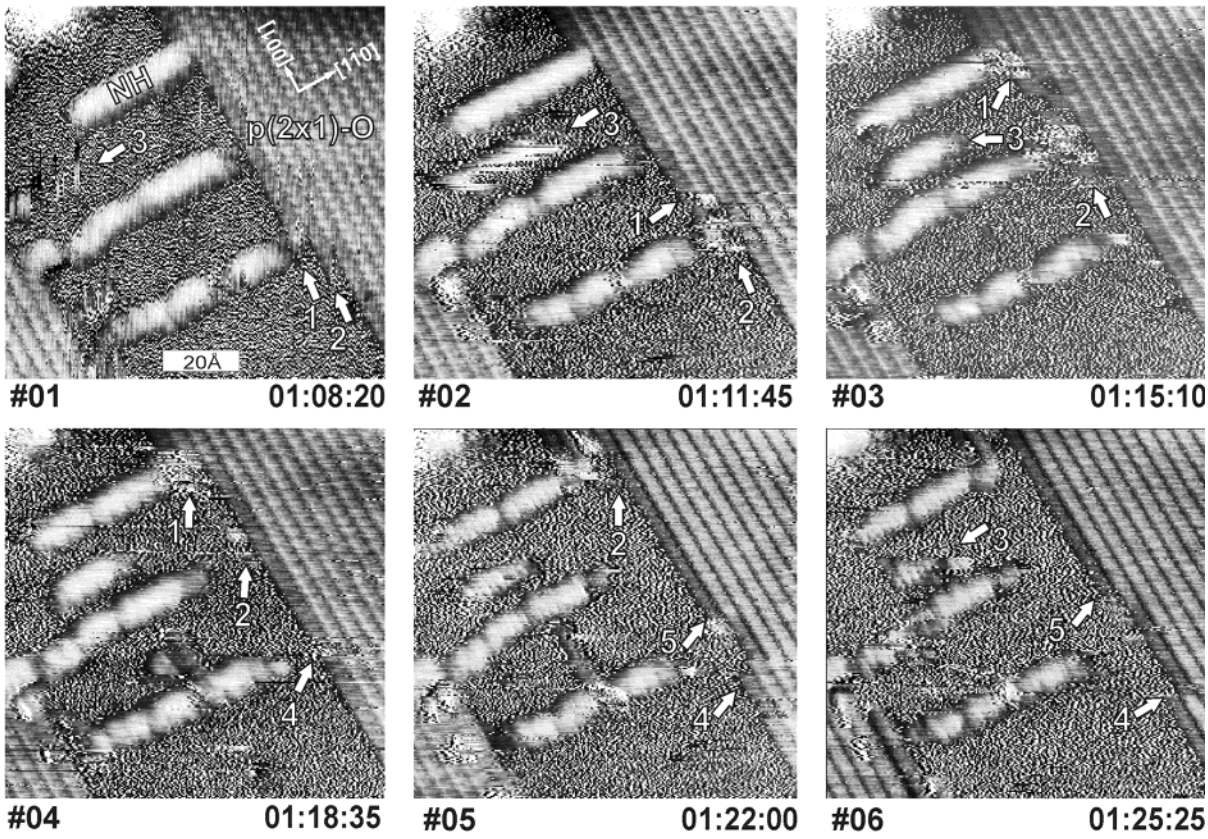

Figure 7. Sequential STM images obtained at 300 K showing the reaction of −Cu−O− rows from the p(2 × 1)-O islands with ammonia on Cu(110).[32] (Section 4.3.) Reproduced with permission of Elsevier. Copyright 1997.

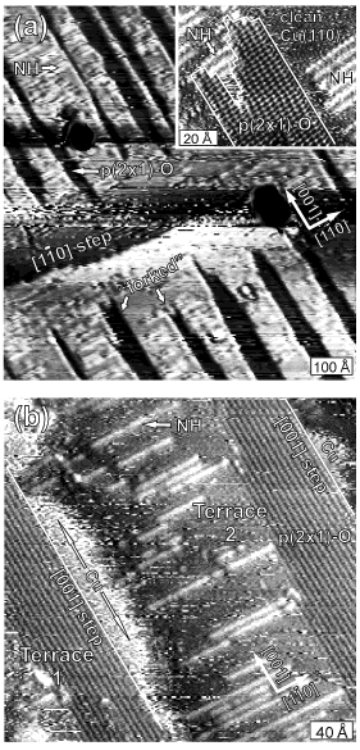

Figure 8. STM images taken at 300 K after heating a coadsorbed layer of NH_3 and O(a) on Cu(110) to 410 K. (a) A large section of the surface with a monatomic [110] step. The inset shows the intrusion of NH rows into the end of an oxygen band. (b) Terraces separated by [001] steps of monatomic height.[33] (Section 4.4.) Reproduced with permission of Elsevier. Copyright 1996.

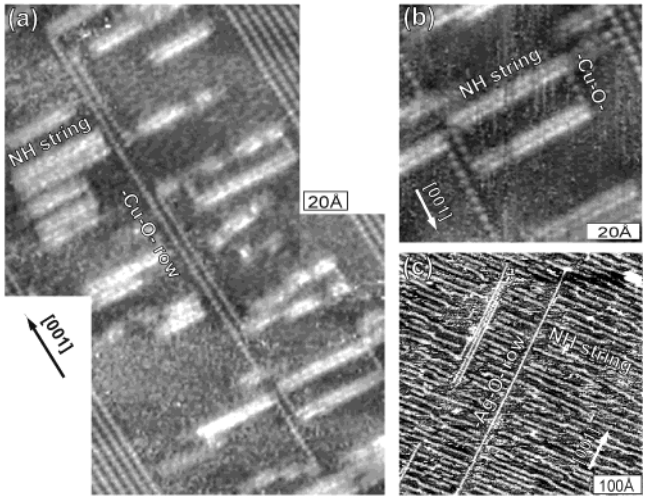

Figure 9. (a) STM image of complex two-dimensional configurations formed by −Cu−O− rows and NH(a) structures after annealing coadsorbed NH_3 + O on Cu(110) to 410 K.[6] Reproduced with permission of the Royal Society of Chemistry. Copyright 1997. (b) STM image after NH_3 exposure on Ag(110)-p(2 × 1)-O at 300 K.[34] (Section 4.5) Reproduced with permission of Elsevier. Copyright 2002.

are also seen to be stabilized by the termination of −Cu−O− rows by rows of NH(a). Rectangular enclosures are formed by two short −Cu−O− rows and two NH(a) structures (Figure 9b). Figure 9c is an STM image after NH_3 exposure on Ag-(110)-p(2 × 1)-O at 300 K. In this case a single −Ag−O− row, about 530 Å long, is stabilized due to blocking of the terminal O(a) by NH(a) strings.

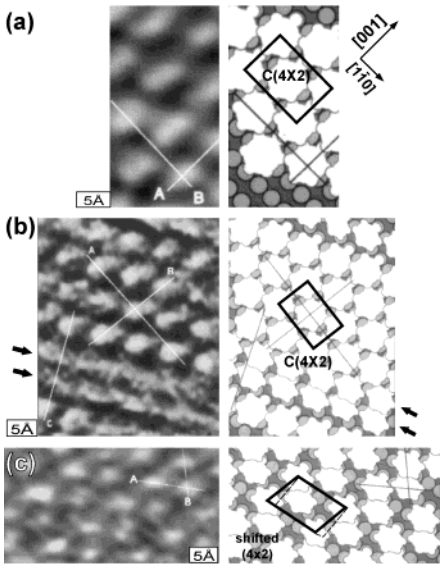

Figure 10. STM images showing three types of structures of phenoxy formed by reaction of phenol with Cu(110).[36] Increasing coverage drives the phenoxy into a more upright configuration. The phenoxy moieties are drawn with their van der Waals sizes. (Section 5.1.) Reproduced with permission of Elsevier. Copyright 1995.

These highly organized stable structures are obviously the result of the interplay of anisotropic reactivity and inhibition effects on reactivity due to site-blockings. Apparently, no oxygen atoms are "intrinsically unreactive" with NH_3 at this temperature, contrary to previous suggestions.[35] The site-blocking inhibition renders the otherwise reactive oxygen rows unreactive.

5. Reaction-Produced Multiphase Structures of Mixed Adsorbates

Locally ordered structures are formed following the reactive adsorption of a number of molecules, including phenol, SO_2, NH_3, and NO_2. Due to the random distribution of these mixed patches, i.e., the lack of long-range order, traditional diffraction techniques, such as low energy electron diffraction (LEED), do not reveal these structures, which are easily resolvable using STM.

5.1. Three Coexisting Structures of Phenoxy from Phenol on Cu(110).[36] It is commonly assumed that on a single-crystal plane adsorbates form a unique two-dimensional structure at a given temperature and pressure. Indeed, a sharp LEED pattern characteristic of a well-defined c(4 × 2) structure is observed for a phenoxy monolayer on Cu(110). However, STM at molecular-scale resolution reveals three different overlayer structures in this monolayer. After a saturation exposure of the clean Cu(110) surface to phenol at 300 K, most regions on the flat terrace exhibit well-ordered structures (Figure 10a). The distance between adjacent protrusions is 7.2 and 10.2 Å, respectively, in the two orthogonal directions indicated by the white lines A and B. These distances correspond to the c(4 × 2) structure shown by the schematic model on the right.

A second regular structure appears in other areas on the same surface (Figure 10b). These structures consist of c(4 × 2) regions interspersed among more densely packed phenoxy chains (marked by arrows). The chains are separated by 4.4 Å. Based on space requirements, this suggests that the phenoxy species in the chains tilt upward away from the surface compared to those in the c(4 × 2) structure. A structure model is illustrated on the right. In forming the chains, the oxygen atoms in phenoxy appear to shift to next nearest neighbor atop sites. The two phenoxy chains form a boundary between two antiphase c(4 × 2) domains.

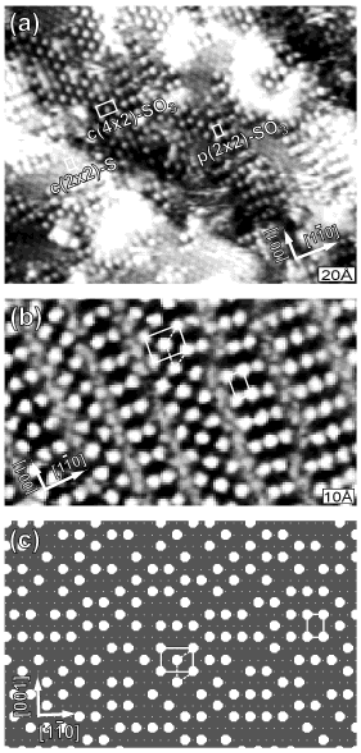

Figure 11. (a) STM image of mixed S and SO_3 structures from SO_2 on Cu(110), and (b) STM image of two equivalent SO_3 structures.[39] (c) A section of the Monte Carlo simulation result showing the equivalent c(4 × 2) and p(2 × 2) arrangements. (Section 5.2.) Reproduced with permission of the American Institute of Physics. Copyright 2002.

Figure 10c displays yet another structure found in the phenoxy monolayer on the same surface. This densely packed phase is similar to that of the double chains shown in Figure 10b. There is no c(4 × 2) arrangement observed within the domain of this structure. The double chains are found throughout the region. The dimensions in this structure are consistent with the model shown on the right. The structure, invisible in LEED, may be considered to be a distorted or shifted c(4 × 2) structure produced by a shift along the [1$\bar{1}$0] direction.

The three structures of the phenoxy moieties observed within the phenoxy monolayer on Cu(110) suggest a preference for maintaining a particular binding site (e.g., atop site). The orientation with respect to the underlying surface varies for the different structures because of differing local density of the phenoxy overlayer; some of the phenoxy are bound nearly parallel to the surface and some are almost normal to the surface. A molecular orientation determined by any technique that samples all orientations is bound to be an average of these three orientations. Such an effect may be the origin of the 15°−20° tilt reported for phenoxy on Pd(110) [37] and Ni(110).[38]

5.2. Mixed S and SO_3 Structures from SO_2 Disproportionation on Cu(110).[39] The exposure of a clean Cu(110) surface to SO_2 results in disproportionation to form adsorbed S and SO_3. Following an exposure of the clean Cu(110) surface to SO_2 at 300 K, STM reveals three local structures: c(2 × 2), c(4 × 2), and p(2 × 2) (Figure 11a). The corrugation of the species comprising the c(2 × 2) domains is smaller than that of the c(4 × 2) and p(2 × 2) structures. However, only the c(2 × 2) structure is observed by LEED. The same c(2 × 2)

structure is produced from the decomposition of H_2S on Cu(110).[40,41] The c(2 × 2) structures are thus believed to be due to the aggregation of the sulfur released in the disproportionation reaction.

Not only do S(a) and SO_3(a) segregate, but SO_3(a) itself appears to adopt two different structures. A mixture of c(4 × 2) and p(2 × 2) structures produced on a large terrace of the clean Cu(110) is shown in Figure 11b. The species comprising the c(4 × 2) and p(2 × 2) structures have identical corrugation. The c(4 × 2) unit cell can be thought of as a distorted "(2 × 2)", one side of which is shifted by one lattice unit along the [001] direction (dash lines). The two structures have the same local coverage of 0.25 ML. The number of shifted "(2 × 2)" structures counted in a large STM image is approximately equal to those of p(2 × 2). A computer simulation implementing a random population of the next nearest neighboring sites yields the same number of shifted "(2 × 2)" and p(2 × 2) structures. A section of the result is shown in Figure 11(c) for a simulation on a 100 × 100 lattice after 10^9 random attempts. This suggests that the c(4 × 2) and p(2 × 2) structures are equivalent arrangements of the same species. The species is identified as adsorbed sulfite (SO_3) by X-ray photoelectron spectroscopy.[39]

5.3. Different Mixed Structures of N(a) and O(a) Produced by Different Reactions on Ag(110)-p(2 × 1)-O.[34] Generally, one would expect that the distribution of reactive intermediates on a surface would depend on their identity, their surface concentration and the temperature and pressure. However, under transient conditions the structures formed can depend on the initial state of the system, i.e., on the distribution of the precursors to the intermediates. The formation of different mixed adlayers of N and O on Ag(110) resulting from the reactions of oxygen in the p(2 × 1)-O structure with ammonia or NO_2, respectively, serve to illustrate this point. It should be noted that with nitrogen dioxide N(a) and O(a) are generated from a single reactant, whereas with NH(a) and O(a) they are not.

5.3.1. From Reaction with NH_3.[34] Previous results from temperature-programmed reaction spectroscopy and electron energy loss spectroscopy have shown that reaction of ammonia (NH_3) with Ag(110)-p(2 × 1)-O at 300 K produces NH(a), and that heating the surface to 450 K leads to a mixed layer of N(a) and O(a).[42] Figure 12a displays an STM image obtained after the surface was heated to 450 K and cooled to 300 K. Two types of locally ordered structures are visible: strings along the [1$\bar{1}$0] direction, attributed to N(a)-associated structures, and short strings running in the [001] direction and stacked along the [1$\bar{1}$0] direction, attributed to O(a)-associated structures. No distinct LEED pattern was observed for this surface due to the lack of long-range order, yet a high degree of local order is evident. The patches of the ordered structures are distributed on the surface rather randomly, although the top of step edges seem to be preferentially occupied by N(a) structures.

Details of the mixed structures are revealed in Figure 12b. The cross sections of the N(a) structure show that the spacing of the broad features along the [001] direction is close to three lattice units, and the spacing along the row in the [1$\bar{1}$0] direction is close to two lattice units. The structure thus corresponds to a (2 × 3) periodicity. The N(a) structure is identical to that obtained from the adsorption of nitrogen ions on Ag(110) [43] and Cu(110).[44] A double-row model that incorporates added metal atoms was proposed for the latter and is adopted here, as shown in Figure 12c (left).

The cross section of the O(a) structure indicates that the averaged spacing between the thick rows is close to 3 lattice

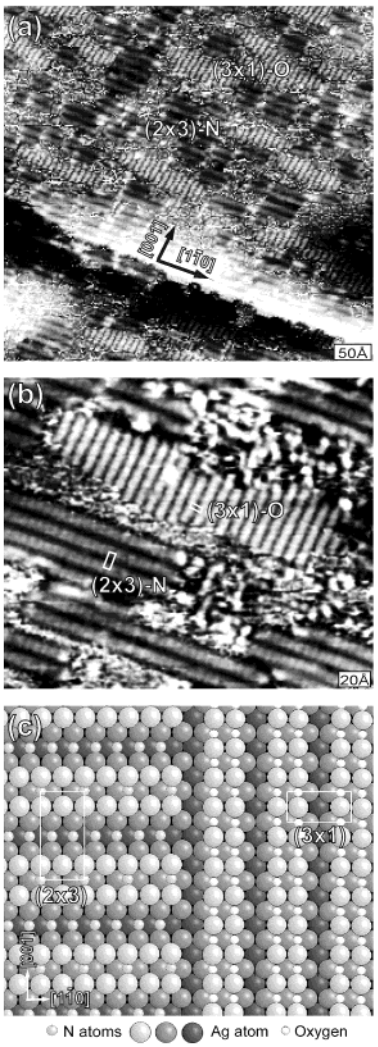

Figure 12. (a) STM image of a mixed layer of N(a) and O(a) formed from NH_3 reaction on Ag(110)-p(2 × 1)-O, and (b) shows more details. The nitrogen appears to compress the oxygen into an unusual structure. (c) A structure model proposed for the mixed layer.[34] (Section 5.3.1.) Reproduced with permission of Elsevier. Copyright 2002.

units. However, the thick O(a) rows are too broad to be attributed to the usual p(3 × 1) single added −Ag−O− row structure.[8] A double added row model is therefore suggested in Figure 12c on the right. The double row structure could be formed from the compression of the p(2 × 1)-O row structures by the N(a) structures. In fact, p(2 × 1)-O rows do occasionally appear in the patches of this p(3 × 1) structure. The presence of the (2 × 3)-N structure appears to induce the formation of an otherwise unstable oxygen structure.

5.3.2. From Reaction with NO_2.[45] Adsorption of NO_2 on Ag(110)-p(2 × 1)-O leads to the formation of surface nitrate (NO_3), as shown previously by TPRS and HREELS.[46] Heating the surface to 480 K produces coadsorbed N(a) and O(a). The STM images of this coadsorbed layer is shown in Figure 13a, which was acquired at 300 K after cooling from 480 K. Clearly this structure is quite different from that formed by reaction of O(a) with ammonia. Regularly spaced zigzag rows are observed to cover the surface. Nowhere are the structures pictured in Figure 12b observed. The length of a straight section in the zigzag rows varies. A more highly resolved image of a small section is shown in the inset. The corresponding cross sections A and B show that the averaged spacing along the row is about one lattice unit along the diagonal of the clean Ag(110)−(1 × 1)

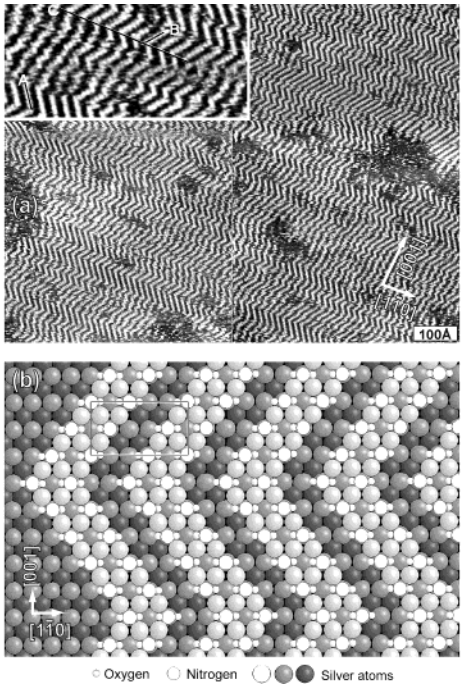

Figure 13. (a) STM image of a mixed layer of N(a) and O(a) formed from NO_2 reaction on Ag(110)-p(2 × 1)-O, and the inset shows more details. (b) A structure model proposed for the mixed layer.[45] Oxygen and nitrogen atoms appear to be utilized cooperatively in the formation of this structure. (Section 5.3.2.) Reproduced with permission of Elsevier. Copyright 2002.

unit cell. The cross section C along the [1$\bar{1}$0] direction yields an averaged spacing close to five lattice units.

The model proposed for this mixed N and O structures is depicted in Figure 13b. The structure consists of short −Ag−O− rows along the [001] direction coupled by interactions with N adatoms. N(a) and O(a) are incorporated into a mixed structure, in contrast to the model proposed for N(a) and O(a) resulting from heating NH(a) and O(a). The 1:2 ratio of N(a) to O(a) is taken from TPRS results.[45] The association of these oxygen atoms with an N(a) adatom is consistent with their observed lack of reactivity with CO.[45] The short −Ag−O− rows sit next to each other, as they are bonded together by N(a) at every oxygen atom. Because of the closer packing compared to the p(2 × 1)-O structure, these −Ag−O− rows are very short, ranging from two to four Ag or O atoms. This arrangement generates naturally the zigzag structure consistent with the dimensions obtained in the STM images.

6. Evidence for Stoichiometric Incorporation of Added Metal Atoms into the Structures of Molecular Intermediates: Nanorestructuring of the Dynamic Surface

Though the traditional view of a rigid surface as a truncation of the bulk has evolved into a "flexible surface" where atomic scale restructuring occurs upon adsorption, it is now clear that surface restructuring is not limited to local rearrangements over the length scale that is a fraction of the lattice constant. Reactions can dramatically alter the surface landscape on a much larger scale, atomically roughening flat regions of the surface as the result of the mass transport of metal atoms in order to stabilize the adsorbed reaction intermediates. Thus, the surface is not just flexible, it is quite dynamic. The surface topography can be altered as surface atoms are incorporated into the unit cells of the adsorbed species on top of the underlying surface. The surface alteration manifests itself as the formation of randomly distributed, nanometer-sized islands or pits on an otherwise flat terrace. These nanometer features are invisible using LEED or other diffraction techniques, but can be easily seen with STM. Such nanorestructuring has been observed for a number of systems where reaction intermediates incorporate additional substrate atoms. The intermediates studied so far include NH-(a), NO_3(a), and SO_3(a) on Ag(110), and SO_3(a) on Cu(110). A well-defined stoichiometry of the unit cell containing the intermediate and the additional metal atoms is suggested by the coverage of the islands or pits. If no stable intermediate is formed in the reaction, e.g. in CO oxidation on Cu(110) (Section 4.2), no islands or pits are formed on the surface.

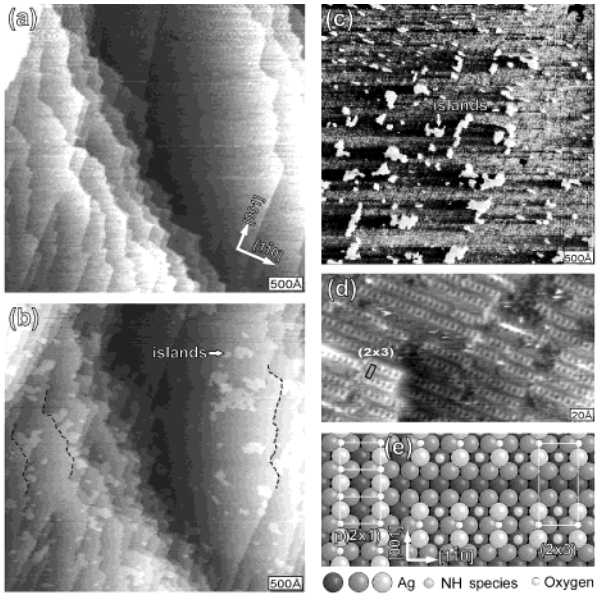

Figure 14. A large-scale STM image of the Ag(110)-p(2 × 1)-O surface before (a) and after (b) ammonia exposure at 300 K. (c) A large-scale STM image of a large terrace after NH_3 exposure. (d) A close-up STM image of the surface. (e) A structure model of the surface before (left) and after (right) NH_3 exposure.[34] (Section 6.1.) Reproduced with permission of Elsevier. Copyright 2002.

6.1. Island Formation from NH_3 on Ag(110)-p(2 × 1)-O.[34] As noted above, to study the structures of surface-bound reaction intermediates by STM, a number of experimental methods must first be used to establish the identity of the species. Temperature programmed reaction spectroscopy and vibrational spectroscopy have been utilized to prove that the reaction of ammonia with the oxygen-covered Ag(110) surface at 300 K produces NH-(a), coadsorbed with residual adsorbed oxygen.[47] A typical, large-scale STM image of the Ag(110)-p(2 × 1)-O surface is shown in Figure 14a for a total oxygen coverage of 0.4 ML. It shows a region consisting of bunched, kinked steps interspersed between a few large (110) terraces several thousand Ångstroms across. After ammonia exposure at 300 K the step edges (dashed lines) become extended and roughened (Figure 14b). Irregularly shaped islands of monatomic height also form on the terraces.

A large-scale STM image of a large terrace after NH_3 exposure is shown in Figure 14c. The islands (white) on the terrace cover ∼12% of the whole area. Prior to reaction with ammonia the p(2 × 1)-O bands cover 75% of the surface, the rest being clean surface. Since ammonia does not adsorbed on clean Ag(110),[48] the island coverage formed from NH_3 on Ag-(110)-p(2 × 1)-O is therefore 16% or, in whole numbers, 1/6 ML.

A close-up image of the surface in Figure 14d shows that double strings with a (2 × 3) structure cover the entire surface, including the extended steps and the newly formed islands. A number of factors are combined in order to suggest a reaction stoichiometry and a structure model. On the bases of HREELS data, NH(a) is formed after ammonia exposure at 300 K.[47] The STM image show that the NH(a) induces a (2 × 3) periodicity. Further, the reaction releases about 1/6 of the added Ag atoms in the p(2 × 1)-O structure, suggesting that there is a net loss of silver from a (2 × 3) cell of the oxygen overlayer. Last, TPRS results demonstrate that part of the oxygen remains on the surface in the form of OH(a) and/or O(a), which evolve as H_2O and NO at higher temperatures. Therefore the following reaction is suggested to occur at 300 K:

$$2NH_3(g) + \{3O(a) + 3Ag(a)\} \rightarrow \{2Ag(a) + 2NH(a) + O(a)\} + Ag(s) + 2H_2O(g) \quad (1)$$

where Ag(a) refers to silver atoms incorporated into the unit cell of the adsorbed species, and Ag(s) refers to freed silver atoms on the surface (islands). A structure model which is consistent with the above observation is depicted in Figure 14-(e), where the (2 × 3) unit cell contains two added Ag atoms and one O atom. In the model the 4-fold hollow binding site is chosen for NH(a) in order to maximize its coordination. Two equivalent 2-fold sites also exist within the unit cell as alternative sites for NH(a). Clearly, further work is needed to establish whether this structure is correct, but it seems apparent that the structure at this stage of the oxidation reaction contains two silver atoms per unit cell.

6.2. Pit Formation from NO_2 on Ag(110)-p(2 × 1)-O.[45] If the intermediate produced by reaction of a species with the p(2 × 1)-O structure on Ag(110) incorporates fewer added silver atoms than the (2 × 1)-O structure itself, islands will be formed from the silver atoms released. On the other hand, if the intermediate incorporates more silver atoms into its unit cell, additional silver atoms must be acquired. These metal atoms can come either from step edges or from terraces. Formation of surface nitrate, NO_3(a), by the reaction of NO_2 with Ag-(110)-p(2 × 1)-O above 300 K[46] is accompanied by the formation of many irregularly shaped pits on the terraces and "fingers" along steps. Figure 15a displays a large-scale STM image of a region of the surface following an NO_2 exposure of the Ag(110)-p(2 × 1)-O surface at 320 K (total initial oxygen coverage was about 0.4 ML). The pits and fingers suggest a substantial migration of silver atoms into the nitrate structures. Quantitative analysis of a larger terrace showed that the pits cover about 18% of the surface. Further magnification reveals thick irregular rows covering 87% of the surface, including the bottom of the large pits (a small section is shown in Figure 15b). These rows are attributed to the surface nitrate species. The spacing between the rows is six lattice units.

The structure proposed for the surface nitrate at high nitrate coverage was based on the STM images obtained at lower nitrate coverage (Figure 15c). This image reveals bright double rows, bright single rows, and dimmer single rows. The dimmer rows are attributed to intervening −Ag−O− rows, while the bright single and double rows are attributed to surface nitrate. Cross sections along the [1$\bar{1}$0] direction (not shown) yield (4 × 1) and (6 × 1) periodicity among single and double rows, respectively. Figure 15d depicts the structures for the single and double nitrate rows as well as the intervening −Ag−O− rows. Since vibrational spectroscopy suggests that the NO_3 possesses a monodentate configuration with C_{2v} symmetry,[46] we propose

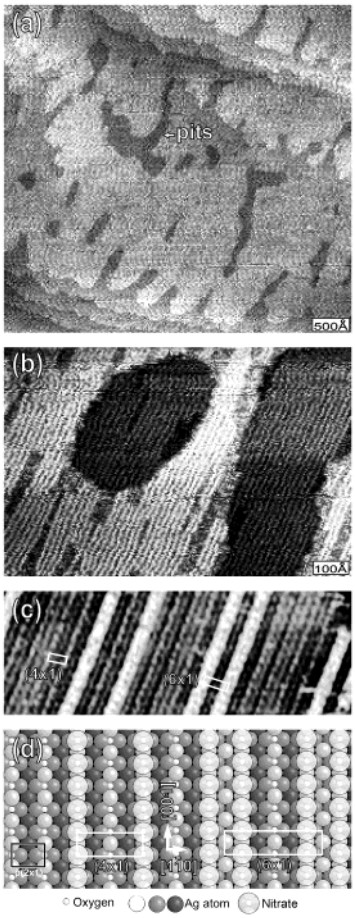

Figure 15. (a) A large-scale STM image following an NO_2 exposure of the Ag(110)-p(2 × 1)-O surface at 320 K. (b) A section of an STM image with further magnification. (c) An STM image of the surface at low nitrate coverage. (d) A structure model of the surface covered by oxygen (left) and both oxygen and nitrate at low (middle) and high (right) nitrate coverage.[45] (Section 6.2.) Reproduced with permission of Elsevier. Coyright 2002.

that it forms by addition of the NO_2 directly on top of an oxygen atom in the (2 × 1) structure. One additional Ag atom is incorporated into each unit cell in the center of the double row in the (6 × 1) structure to account for the 18% pit formation on the terrace. Thus the overall reaction, which acquires silver atoms from the surface, appears to be

$$2NO_2(g) + \{3O(a) + 3Ag(a)\} + Ag(s) \rightarrow \{4Ag(a) + 2NO_3(a) + O(a)\} \quad (2)$$

A detailed mass balance for O(a) and added Ag atoms for the whole surface has been reported elsewhere.[45]

6.3. Island Formation from SO_2 on Ag(110)-p(2 × 1)-O.[49] At 300 K sulfur dioxide reacts with oxygen on Ag(110) to form a surface sulfite (SO_3(a)) in a c(6 × 2) arrangement, as found previously using XPS, UPS, TPRS, LEED, and HREELS.[50−53] The surface was imaged with STM following SO_2 exposure on Ag(110)-p(2 × 1)-O at 300 K. A section of a large area scan (Figure 16a) shows a large terrace covered with scattered islands of monatomic height and of diameters ranging from 10 to 40 nm, covering about 13% of the surface. The initial state of the Ag(110)-p(2 × 1)-O surface is 75% covered by the p(2 × 1)-O bands. The island coverage formed from the reaction of SO_2 on Ag(110)-p(2 × 1)-O due to the release of silver atoms from the p(2 × 1)-O structure is therefore 1/6 ML.

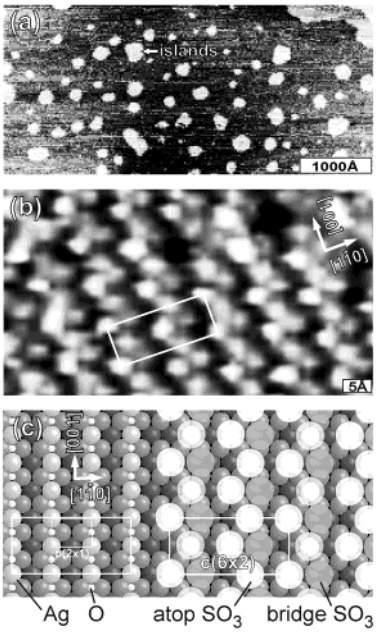

Figure 16. (a) A section of an STM image following SO_2 exposure on Ag(110)-p(2 × 1)-O at 300 K. (b) A zoom-in STM image of the sulfite-covered surface. (c) A structure model of the surface before (left) and after (right) SO_2 exposure.[49] (Section 6.3.) Reproduced with permission of Elsevier. Copyright 2002.

A zoomed-in STM image of the sulfite-covered surface shows the c(6 × 2) periodicity (Figure 16b). Four of the six protrusions in the unit cell are of higher corrugation than the other two. Consistent with the extent of island formation, we propose that the sulfite species have two different local environments with respect to the added silver atoms, as depicted in Figure 16c. The 1/2 ML of added silver atoms in the p(2 × 1)-O structure are redistributed after the sulfite formation, and one-third of them are incorporated into the c(6 × 2)-SO_3 structure, freeing 1/6 ML to form islands. The overall reaction can be written as

$$6SO_2(g) + \{6O(a) + 6Ag(a)\} \rightarrow \{4AgSO_3(a) + 2SO_3(a)\} + 2Ag(s) \quad (3)$$

We propose that the brighter features in the STM image (Figure 16b) result from sulfite bound atop added silver atoms in a 4-fold hollow site. The dimmer features are due to sulfite with no added silver atom underneath in a long-bridge site.

6.4. Pit Formation from SO_2 on Cu(110).[39] A large-scale image resulting from the reaction of SO_2 with clean Cu(110) at 300 K is shown in Figure 17a. X-ray photoelectron spectroscopy shows that SO_2 disproportionates according to

$$3SO_2(g) \rightarrow S(a) + 2SO_3(a) \quad (4a)$$

The image reveals that exposing SO_2 to the clean surface with flat terraces produces pits of monatomic height (black dots), which cover about 18% of the surface. Closer examination reveals S(a) in a c(2 × 2) structure and sulfite in both a p(2 × 2) and a c(4 × 2) structure (cf. Figure 11b). Since the formation of the same c(2 × 2)-S structure from H_2S does not create pits on Cu(110),[40,39] the pit formation is due to the formation of the sulfite species.

The relative areas covered by c(2 × 2)-S and SO_3 are determined directly from STM images away from the pits. A typical image is shown in Figure 17b. An average of 15 images over different regions indicates that 80% of the surface is covered by SO_3(a). The local coverage within the p(2 × 2) or

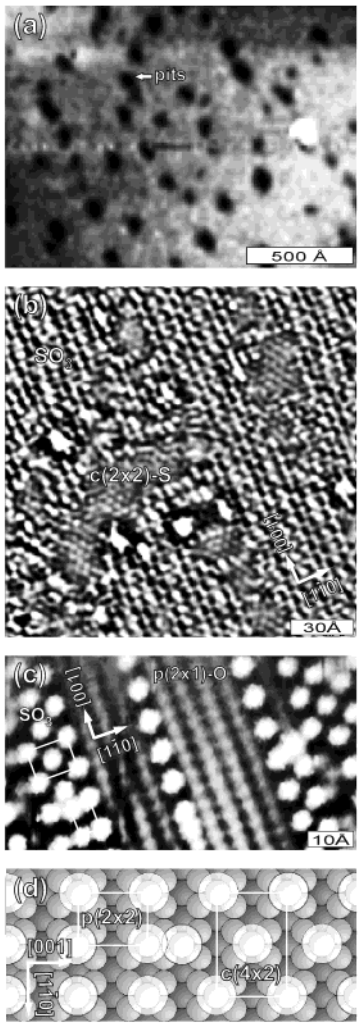

Figure 17. (a) A large-scale STM image resulting from the reaction of SO_2 with clean Cu(110) at 300 K. (b) A zoom-in STM image showing mixed sulfur and sulfite structures. (c) A structure model of the sulfite structures.[39] (Section 6.4.) Reproduced with permission of the American Institute of Physics. Copyright 2002.

c(4 × 2) unit cell is 0.25 ML. Therefore, the overall SO_3(a) coverage is 0.20 ML. Similarly, the overall S(a) coverage is 0.10 ML. Thus, the ratio of S(a) to SO_3(a) determined by STM is 1:2, which agrees with the XPS results.[39] The pit coverage (0.18 ML) indicates that the formation of one SO_3(a) incorporates one Cu atom. Reaction 4a becomes

$$3SO_2(g) + 2Cu(s) \rightarrow S(a) + 2CuSO_3(a) \quad (4b)$$

On the bases of these observations and consistent with an STM image (Figure 17c) of mixed SO_3(a) and O(a), a structural model proposed is displayed in Figure 17c. The sulfite species binds through an oxygen atom atop an added Cu atom. The monodentate configuration is suggested from isotopic exchange results.[39]

7. Summary

The application of scanning tunneling microscopy to the study of surface reactions has revealed a number of important characteristics that influence surface reactivity. Coadsorbed reactants, or reactants and metastable reaction intermediates, can form highly organized, interactive structures that strongly affect their reactivity. In some cases these structures may actually inhibit reaction. Further, these structures may exhibit

pronounced structural anisotropy in their reactivity on surfaces of low symmetry. With near defects, such as step defects, reactivity may be altered, but even on large terraces adsorbates may form a number of different phases of differing reactivity at a given temperature and pressure. These differing structures can originate from a mechanistically different pathway to the given coverage of each species or from local inhomogeneities in surface concentration. Last, a metal surface is dynamic, consisting of terraces, steps, kinks, and mobile atoms in equilibrium. These mobile atoms make the surface a dynamic entity, and they can be incorporated into the structures of adsorbed reaction intermediates, thereby affecting their stability and reactivity.

Acknowledgment. Support of the National Science Foundation through grants NSF CHE 9400526 and CHE 9820703 is gratefully acknowledged.

Note Added after ASAP Posting. This paper was posted on 2/01/2003 without copyright information in the figure captions. The corrected paper was posted 3/12/2003.

References and Notes

(1) Crew, W. W.; Madix, R. J. *Rev. Sci. Instrum.* **1995**, *66*, 4552.
(2) Somorjai, G. A. *Langmuir* **1991**, *7*, 3176.
(3) Guo, X.-C.; Madix, R. J. *Acc. Chem. Res.*, in press.
(4) Madix, R. J.; Biener, J.; Baumer, M.; Dinger, A. *Faraday Discuss.* **1999**, *114*, 67.
(5) Guo, X.-C.; Madix, R. J. *J. Phys. Chem. B* **2001**, *105*, 3878.
(6) Guo, X.-C.; Madix, R. J. *J. Chem. Soc., Faraday Trans.* **1997**, *93*, 4197.
(7) Wintterlin, J.; Schuster, R.; Coulman, D.; Ertl, G.; Behm, R. J. *J. Vac. Sci. Technol. B* **1991**, *9*, 902.
(8) Taniguchi, M.; Tanaka, K.; Hashizume, T.; Sakurai, T. *Surf. Sci.* **1992**, *262*, L123.
(9) Pai, W. W.; Reutt-Robey, J. E. *Phys. Rev. B* **1996**, *53*, 15977.
(10) Guo, X.-C.; Madix, R. J. *Surf. Sci.* **2001**, *489*, 37.
(11) Bowker, M.; Barteau, M. A.; Madix, R. J. *Surf. Sci.* **1980**, *92*, 528.
(12) Barteau, M. A.; Madix, R. J. *J. Chem. Phys.* **1981**, *74*, 4144.
(13) Stuve, E. M.; Madix, R. J.; Sexton, B. A. *Chem. Phys. Lett.* **1982**, *89*, 48.
(14) Barteau, M. A.; Madix, R. J. *J. Electroanal. Chem. Interfacial Electrochem.* **1983**, *31*, 101.
(15) Backx, C.; Degroot, C. P. M.; Biloen, P.; Sachtler, W. M. H. *Surf. Sci.* **1983**, *128*, 81.
(16) Campbell, C. T.; Paffett, M. T. *Surf. Sci.* **1984**, *143*, 517.
(17) Prince, K. C.; Bradshaw, A. M. *Surf. Sci.* **1983**, *126*, 49.
(18) Prince, K. C.; Paolucci, G. *J. Electroanal. Chem. Interfacial Electrochem.* **1985**, *37*, 181.
(19) Ricken, D. E.; Somers, J. S.; Robinson, A. W.; Bradshaw, A. M. *J. Chem. Phys.* **1991**, *94*, 8592.
(20) Constant, L.; Krenzer, B.; Stenzel, W.; Conrad, H.; Bradshaw, A. M. *Surf. Sci.* **1999**, *428*, 262.
(21) Krenzer, B.; Constant, L.; Conrad, H. *J. Chem. Phys.* **1999**, *111*, 1288.
(22) Krenzer, B.; Constant, L.; Conrad, H. *Surf. Sci.* **1999**, *443*, 116.
(23) Stensgaard, I.; Laegsgaard, E.; Besenbacher, F. *J. Chem. Phys.* **1995**, *103*, 9825.
(24) Okawa, Y.; Tanaka, K. *Surf. Sci.* **1995**, *344*, L1207.
(25) Pai, W. W. Ph.D. Dissertation, Unversity of Maryland, 1995.
(26) Au, C. T.; Roberts, M. W. *J. Chem. Soc., Faraday Trans.* **1987**, *83*, 2047.
(27) Crew, W. W.; Madix, R. J. *Surf. Sci.* **1996**, *456*, 1.
(28) Crew, W. W.; Madix, R. J. *Surf. Sci.* **1994**, *319*, L34.
(29) Crew, W. W.; Madix, R. J. *Surf. Sci.* **1996**, *349*, 275.
(30) Leibsle, F. M.; Murray, P. W.; Francis, S. M.; Thornton, G.; Bowker, M. *Nature* **1993**, *363*, 706.
(31) Leibsle, F. M.; Francis, S. M.; Davis, R.; Xiang, N.; S., H.; Bowker, M. *Phys. Rev. Lett.* **1994**, *72*, 2569.
(32) Guo, X.-C.; Madix, R. J. *Surf. Sci.* **1997**, *387*, 1.
(33) Guo, X.-C.; Madix, R. J. *Surf. Sci.* **1996**, *367*, L95.
(34) Guo, X.-C.; Madix, R. J. *Surf. Sci.* **2002**, *501*, 37.
(35) Afsin, B.; Davies, P. R.; Pashusky, A.; Roberts, M. W. *Surf. Sci.* **1993**, *284*, 109.
(36) Guo, X.-C.; Madix, R. J. *Surf. Sci.* **1995**, *341*, L1065.
(37) Ramsey, M. G.; Rosina, G.; Steinmuller, D.; Graen, H. H.; Netzer, F. P. *Surf. Sci.* **1990**, *232*, 266.
(38) Bu, H.; Bertrand, P.; Rabalais, J. W. *J. Chem. Phys.* **1993**, *98*, 5855.
(39) Alemozafar, A. R.; Guo, X.-C.; R. J. Madix. *J. Chem. Phys.* **2002**, *116*, 4698.
(40) Carley, A. F.; Davies, P. R.; Jones, R. V.; Harikumar, K. R.; Kulkarini, G. U.; Roberts, M. W. *Surf. Sci.* **2000**, *447*, 39.
(41) Atrei, A.; Johnson, A. L.; King, D. A. *Surf. Sci.* **1991**, *254*, 65.
(42) Thornburg, D. M.; Madix, R. J. *Surf. Sci.* **1989**, *220*, 268.
(43) Moriwaki, K.; Matsumoto, Y.; Ikai, M.; Tanaka, K. *Chem. Phys. Lett.* **1998**, *292*, 500.
(44) Leibsle, F. M.; Davis, R.; Robinson, A. W. *Phys. Rev. B* **1994**, *49*, 8290.
(45) Guo, X.-C.; Madix, R. J. *Surf. Sci.* **2002**, *496*, 39.
(46) Outka, D. A.; Madix, R. J. *Surf. Sci.* **1987**, *179*, 1.
(47) Thornburg, D. M.; Madix, R. J. *Surf. Sci.* **1989**, *220*, 268.
(48) Gland, J. L.; Sexton, B. A.; Mitchell, G. E. *Surf. Sci.* **1982**, *115*, 623.
(49) Alemozafar, A. R.; Guo, X.-C.; Madix, R. J.; Hartmann, N.; Wang, J. *Surf. Sci.* **2002**, *504*, 223.
(50) Outka, D. A.; Madix, R. J. *J. Vac. Sci. Technol.* **1982**, *20*, 882.
(51) Outka, D. A.; Madix, R. J. *Surf. Sci.* **1984**, *137*, 242.
(52) Outka, D. A.; Madix, R. J.; Fisher, G. B.; DiMaggio, C. *J. Phys. Chem.* **1986**, *90*, 4051.
(53) Outka, D. A.; Madix, R. J.; Fisher, G. B.; DiMaggio, C. *Langmuir* **1986**, *2*, 406.